Multi-scale Dynamics of Organic Light-Emitting Devices

A dissertation submitted to the faculty of the graduate school of the University of Minnesota

Kyle William Hershey

In partial fulfillment of the requirements for the degree of Doctor of Philosophy

Russell J. Holmes, Advisor

January 3, 2018

Acknowledgements

I would like to thank my research advisor Russell J. Holmes for all of his guidance and advice.

Parents

Mary Beth

Dow Chemical for funding and collaboration. Dow scientists for research guidance, samples, etc.

Dedication

To some people that I value

Abstract

Over the last decade, organic light-emitting devices (OLEDs) have grown to receive tremendous attention for application in commercial displays and in lighting. While mostly successful for small format displays, challenges still exist that limit their performance for broader applications. Many of these limitations stem from a lack of understanding of charge and exciton dynamics and their impact on efficiency and stability. In this presentation, we describe novel device characterization and modelling efforts aimed at elucidating key dynamic processes in multiple regimes, including the microsecond transient behavior, steady-state, and long term degradation.

A model is presented which unifies both the transient and steady-state electroluminescence behavior of an OLED as a function of current density. The excellent agreement between the model and experiment enables a deeper understanding of efficiency reduction at high brightness. Additionally, the relatively ambiguous device efficiency parameter of charge balance is recast as an exciton formation efficiency. This framework permits a novel characterization paradigm for decoupling degradation pathways during OLED life-testing. In addition to the luminance loss, the degradation in emitter photoluminescence and exciton formation efficiency are also extracted. This technique is applied to an archetypical phosphorescent OLEDs, enabling more comprehensive design rules for device engineering to realize enhanced lifetime. Data science is a rising topic in industrial research. A system for enabling data science techniques within laboratory research is presented. Select useful applications are demonstrated.

Contents

Chapter 1

Overview of Organic Semiconductors

1.1 Organic Semiconductors

1.2 Excitons

1.2.1 Singlets and Triplets

1.2.2 Electronic Transitions

1.3 Charge Transport

Chapter 2

Organic Light-Emtting Devices

2.1 Fabrication Processes

2.2 Characterization

2.2.1 Luminance

2.2.2 Efficiency Analysis

2.3 Historical Developement

2.3.1 The First OLEDs

2.3.2 Phosphorescence

2.3.3 Host-Guest Systems

2.3.4 Cohost Systems

2.3.5 Thermally Activated Delayed Fluorescence

2.4 Device Operation

2.4.1 Dynamic Processes

2.4.2 Efficiency Roll-Off

2.5 Recombination Zone Characterization

2.6 Single Carrier Devices

Chapter 3

Transient and Steady-State Dynamics

This section is referencing my paper.[2, 3]

3.1 Motivation

3.2 Theory

3.2.1 Previous Efficiency Roll-Off Models

3.3 Exciton Dynamics

$$\frac{dn_{ex}}{dt} = -\frac{n_{ex}}{\tau} - \frac{1}{2}k_{TT}n_{ex}^2 - k_{TP}n_{pol}n_{ex} + G_{ex} \tag{3.1}$$

$$G_{ex} = \frac{k_F}{4}n_{pol}^2 \tag{3.2}$$

3.4 Polaron Dynamics

$$\frac{dn_{pol}}{dt} = \frac{-k_F}{2}n_{pol}^2 - \frac{n_{pol}}{\tau_l} + G_{pol} \tag{3.3}$$

3.5 Exciton Quenching in Photoluminescence

$$V = \left[\frac{J}{e\mu N_C} d^{2l+} \left(\frac{eN_0 k_B T_t}{\epsilon}\right)^l\right]^{\frac{1}{l+1}} = CJ^{\frac{1}{l+1}} \tag{3.4}$$

$$n_{pol} = eN_c \left(\frac{\epsilon V}{ed^2 N_0 k T_t}\right)^l \tag{3.5}$$

$$\frac{L(n_{pol}}{L_0} = \frac{1}{1 + \tau k_{TP} n_{pol}} \tag{3.6}$$

3.5.1 Transient Electroluminescence

3.5.2 Efficiency Analysis

$$\eta_{EQE} = \eta_{OC}\eta_{PL}\chi\eta_{EF} \tag{3.7}$$

$$\eta_{EQE} = \frac{\eta_{OC}\eta_{ex}k_r}{G_{pol}/2} \tag{3.8}$$

$$\eta_{EF} = \frac{\frac{1}{2}k_F n_{pol}}{G_{pol}} = \frac{\frac{1}{2}k_F n_{pol}}{\frac{1}{2}k_F n_{pol} + \frac{1}{\tau_l}} \tag{3.9}$$

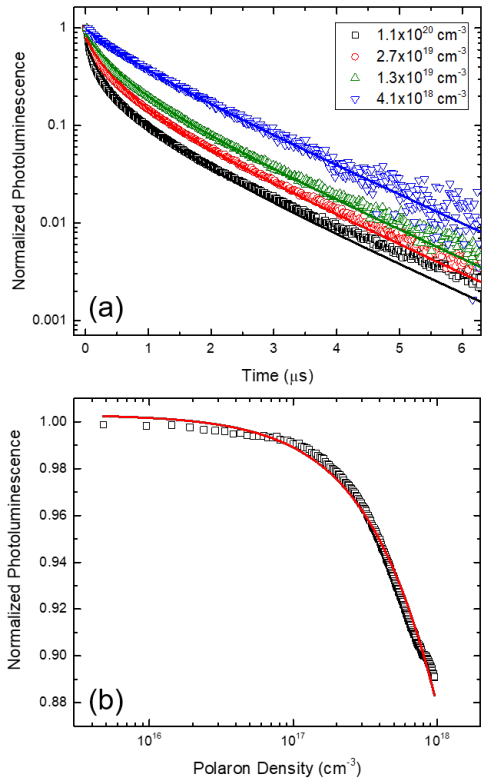

Figure 3.1: (a) Transient photoluminescence (PL) decays for several initial exciton densities with fits shown as solid lines using Eqn. 3.2. Fit parameters are discussed in SECTION. Exciton densities are calculated using measured incident power and beam size in combination iwht Beer's Law. (b) Steady-state PL quenching as a function of polaron density and the resulting fit from Eqn. 3.6 shown as the solid line.

3.6 Experimental Details

3.7 Application to Devices

3.7.1 Overview of Approach

3.7.2 Initializing Parameters with Quenching Only Steady-State Model

3.7.3 Transient Modeling

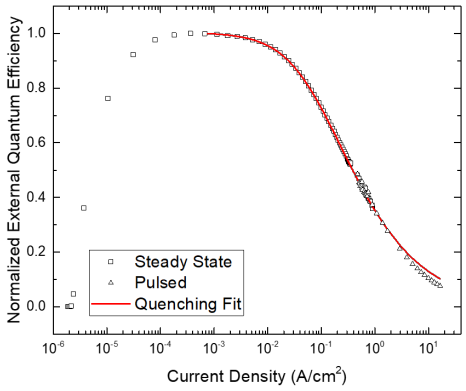

Figure 3.2: Normalized experimental η_{EQE} as a function of current density. Solid line is a fit to the data using Eqn. 3.1 and 3.3 in the absence of polaron loss. Pulsed η_{EQE} measurements are conducted using low duty cycle pulses to steady-state luminance to reduce Joule heating in device.

	Transient EL	Efficiency Roll-off
τ (s)	$6.9 \pm 0.1 \times 10^{-7}$	6.1×10^{-7}
k_{TT} (cm^3/s)	7.1×10^{-12}	7.1×10^{-12}
k_{TP} (cm^3/s)	3.3×10^{-13}	3.3×10^{-13}
k_F (cm^3/s)	$7.7 \pm 3.5 \times 10^{-12}$	1.6×10^{-11}

Table 3.1: Fit parameters extracted from transient and steady-state electroluminescence. Transient EL fit parameters averaged over all measured current densities. η_{EQE} roll-off parameters averaged over several measured devices. Triplet-triplet annihilation and triplet-polaron quenching rates are fixed to those obtained from fitting the normalized efficiency roll-off.

3.7.4 Term Efficiency During Transient

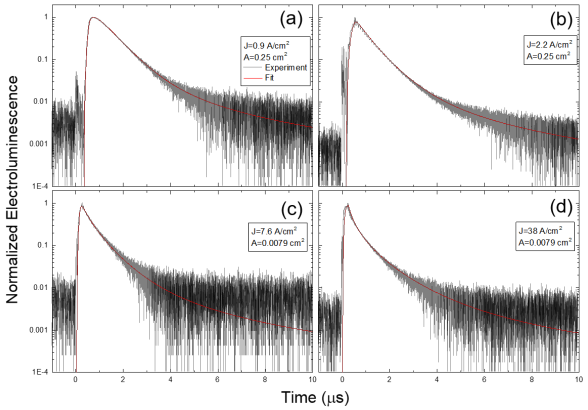

Figure 3.3: Transient electroluminescence (EL) for four different current densities (J) and device areas (A). (a) 0.25 cm^2 device at a current density during the pulse of J = 0.9 A/cm^2 (b) 0.25 cm2 device at J = 2.2 A/cm^2 (c) 0.0079 cm^2 device at J = 7.6 A/cm^2 (d) 0.0079 cm^2 device at J = 38 A/cm^2

3.7.5 Extracting Exciton Formation Efficiency

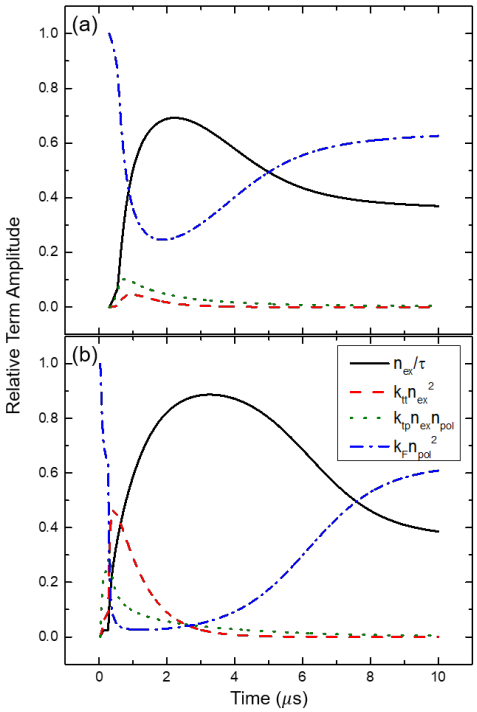

Figure 3.4: Term efficiency for each dynamical process influencing the exciton population for (a) 0.25 cm^2 device operated at 0.9 A/cm^2 for 500 ns and (b) 0.785 mm^2 device operated at a current density of 38 A/cm^2 for 250 ns. Relative term amplitude is calculated as the magnitude of each term in Eqn. 3.1 divided by the sum of absolute values of each term.

$$\tau_l = \frac{w}{E\mu(E)} \tag{3.10}$$

3.8 Understanding Assumptions of Polaron Model

3.8.1 Carrier Injection

$$\frac{dn_h}{dt} = -k_F n_e n_h - \frac{n_h}{\tau_{lh}} + \frac{J_h}{ew} \tag{3.11}$$

$$\frac{dn_e}{dt} = -k_F n_e n_h - \frac{n_e}{\tau_{le}} + \frac{J_e}{ew} \tag{3.12}$$

$$J_1 \rightarrow J_h = J_2 \rightarrow J_e \tag{3.13}$$

$$\frac{J_e}{ew} + \frac{J_h}{ew} = \frac{J_1 + J_2}{ew} = \frac{2J}{ew} \tag{3.14}$$

$$J_1 = J_h \tag{3.15}$$

$$J_2 = J_e + J_l \tag{3.16}$$

$$J = J_h = J_e + J_l \tag{3.17}$$

$$G_{pol} - \frac{J_l}{ew} = \frac{2J - J_l}{ew} \tag{3.18}$$

3.8.2 Charge Imbalance

$$\alpha = \frac{n_h}{n_e + n_h} \tag{3.19}$$

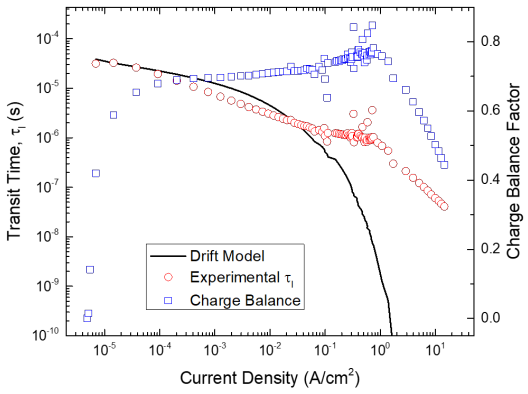

Figure 3.5: Transit time extracted from η_{EQE} measurements are shown as the red circles. Predictions using the drift model are calculated using Eqn. 3.10. The drift model assumes a uniform electric field. Good agreement between the experimental transit time and the drift model is found for a field distributed over 20 nm. The charge balance factor is shown as a function of current density in blue squares.

$$\left[\frac{dn_{pol}}{dt}\right]_{formation} = -2k_F n_{pol}^2 \alpha(1-\alpha) \qquad (3.20)$$

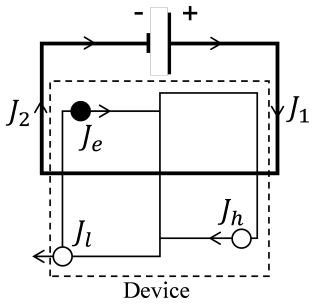

Figure 3.6: Current density formalism within the circuit. and are the currents measured on either side of the device. and are the electron and hole currents within the device and is the unbalanced current, assumed to be only holes, that leaks out of the opposing contact.

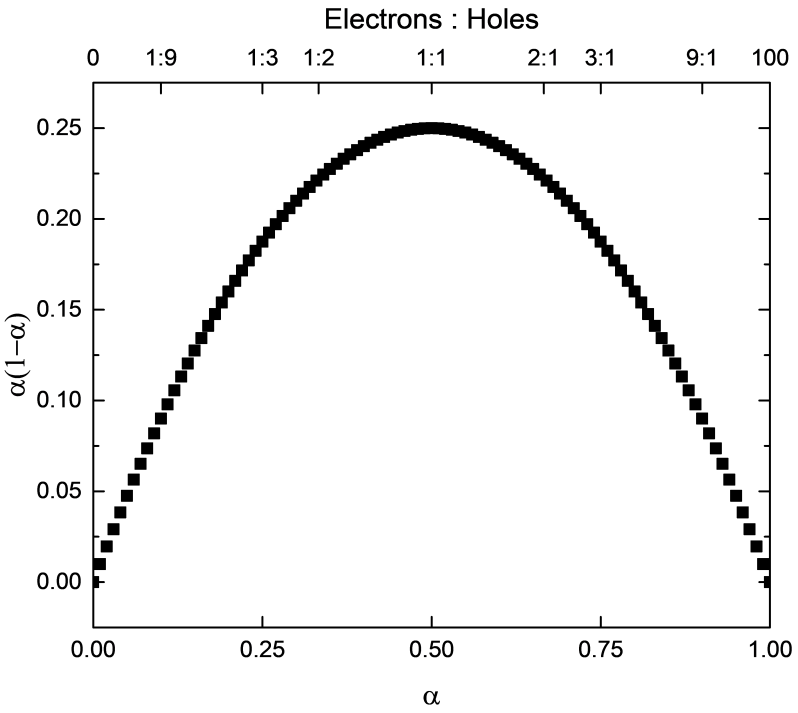

Figure 3.7: The quantity $\alpha(1-\alpha)$ is plotted as a function of the polaron composition, α and the electron to hole ratio.

Chapter 4

Integrated Photoluminescence Lifetimes

4.1 Luminance as Efficiency Loss

$$\eta_{EQE} = \eta_{PL}\eta_{OC}\chi\eta_{EF}\eta_{\tau} \tag{4.1}$$

$$\frac{\eta_{EQE}(t)}{\eta^0_{EQE}} = \frac{\eta_{PL}(t)}{\eta^0_{PL}}\frac{\eta_{EF}(t)}{\eta^0_{EF}} \tag{4.2}$$

4.2 Photoluminescence Characterization

$$\frac{\eta_{PL}(t)}{\eta^0_{PL}} = \frac{L_{PL}(t)}{L^0_{PL}}\frac{I^0}{I(t)} \tag{4.3}$$

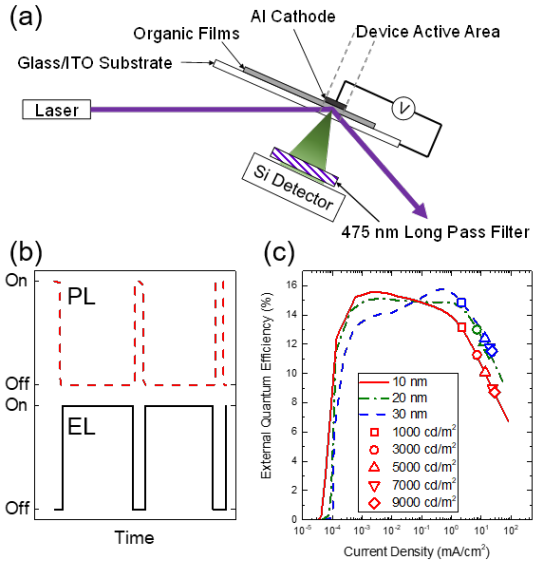

Figure 4.1: (a) Experimental configuration for the measurement of electro- (EL) and photoluminescence (PL) during OLED degradation. Laser excitation is incident on a subsection of the device area. The laser is aligned so that neither the incident nor reflected beam strikes the detector. Stray laser light is removed by a λ=475 nm dielectric long pass filter. (b) Excitation scheme. EL and PL signals are probed independently with no temporal overlap. (c) External quantum efficiency versus current density and luminance for devices having emissive layer thickness of 10 nm, 20 nm and 30 nm.

4.2.1 Light Selection

4.2.2 Absorption - Recombination Overlap

4.2.3 Contact Degradation

4.2.4 Quenching Changes During Degradation

4.2.5 Verification with Excton Lifetime

4.3 Experimental Implementation

4.3.1 Hardware Setup

4.3.2 Software Developement

4.3.3 Database Integration

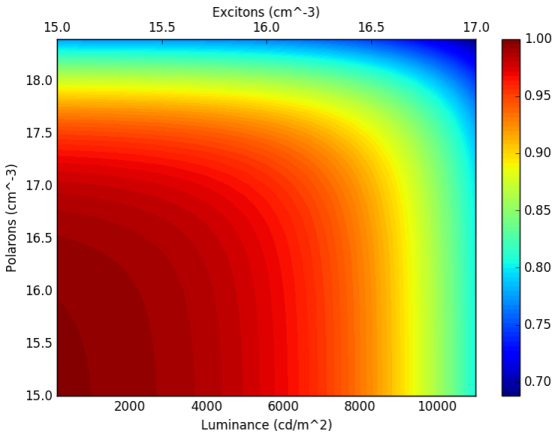

Figure 4.2: Multiplicative correction factor for exciton formation efficiency due to changes in quenching during lifetime. Shown as a function of polaron and exciton density as well as luminance, assuming a 10 nm emissive layer.

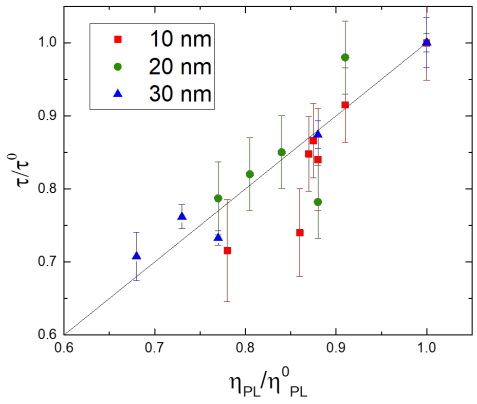

Figure 4.3: Exciton lifetime ratio extracted from transient PL measurements on degraded and undegraded devices as a function of emissive layer thickness.

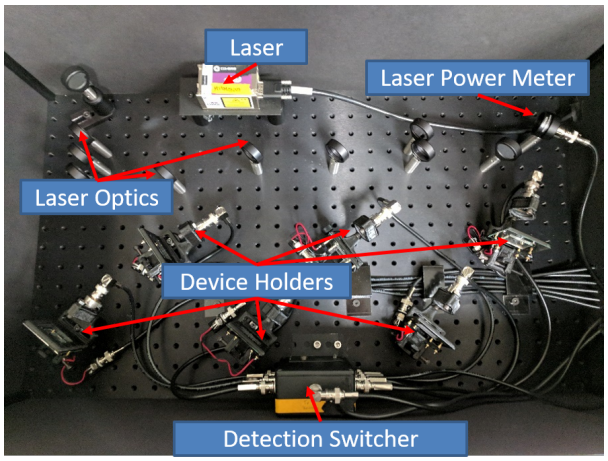

Figure 4.4: Device contacting, measurement, and optical hardware. Version 3 of the hardware is shown. Controlling hardware is shown in Fig. 4.5

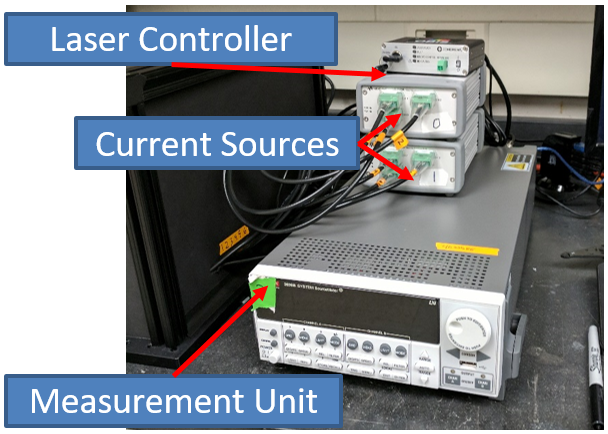

Figure 4.5: Source-Measure hardware and laser controller

Figure 4.6: 6 channel software controller. Selection of test type, laser control for allignment, and global settings are accessible on the top of the interface. Individual channel settings are grouped on the bottom.

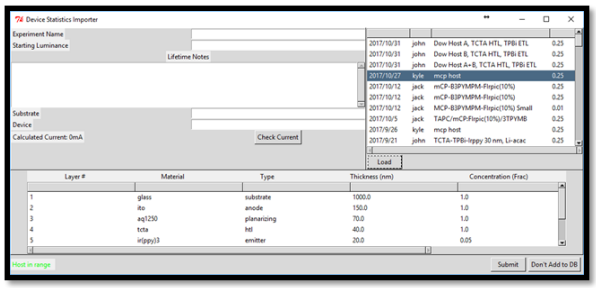

Figure 4.7: Test information for database import interface. The top left panel collects information about the specific device and lifetime. The right panel connects the device to a particular growth and architecture. The bottom panel confirms the architecture.

Chapter 5

Applied Integrated Lifetimes

5.1 CBP Host Thickness

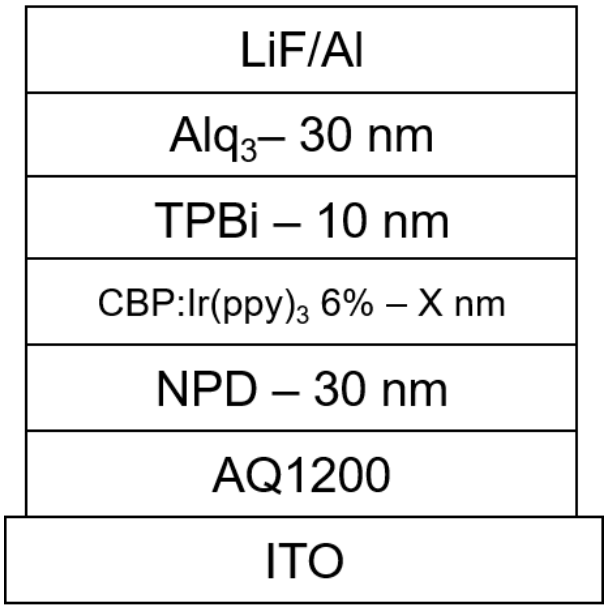

Figure 5.1: Device architecture, featuring EML thicknesses of X=10,20, and 30 nm

5.2 MEML Luminance Scaling

5.3 Dow Cohost

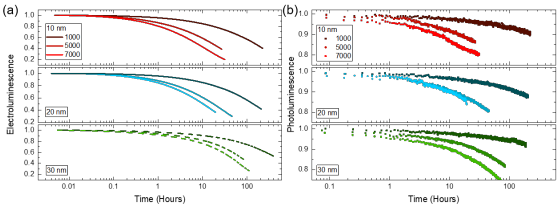

Figure 5.2: Device decay curves for multiple values of the initial luminance as a function of emissive layer thickness. Loss in (a) electroluminescence (EL) and (b) photoluminescence (PL) are shown and decrease monotonically with increasing luminance. For devices with a 10-nm-thick emissive layer, initial luminance values are 1000 cd/m^2, 5000 cd/m^2, and 7000 cd/m^2. For devices with a 20-nm- or 30-nm-thick emissive layer, initial luminance values are 1000 cd/m^2, 5000 cd/m^2, and 7100 cd/m^2.

d_{EML} (nm)	L_0 (cd/m^2)	J (mA/cm^2)	V_0 (V)	t_{50} (hours)
10	1000	2.2	4.2	139.0
	3000	7.2	5.1	39.9
	5000	13.6	5.4	15.8
	7000	14.4	6.2	6.9
	9000	28.0	6.3	5.3
20	1000	2.2	5.4	141.1
	3000	7.2	6.0	33.1
	5000	12.4	7.2	17.2
	7100	19.2	7.3	10.0
	9000	24.0	7.5	8.0
30	1000	2.2	5.9	474
	5000	13.6	7.3	74.4
	7100	19.6	7.6	46
	8000	22.4	7.7	38.1

Table 5.1: Summary of device lifetimes. For each device, the starting luminance (L_0), current density (J), starting voltage (V_0) and time at which 50% of the initial luminance is reached (t_{50}) are reported.

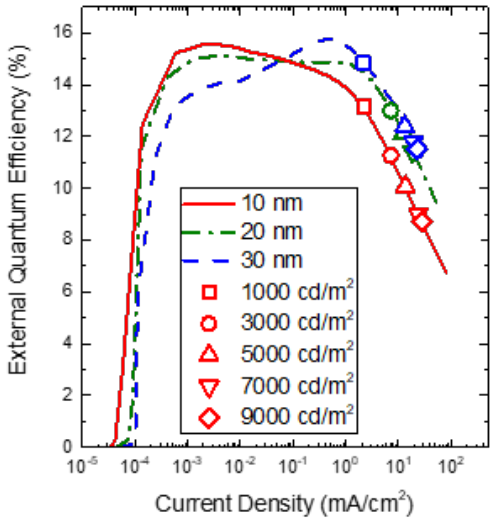

Figure 5.3: External Quantum Efficiency (η_{EQE}) for the three architectures. Operational points for lifetime are shown in symbols.

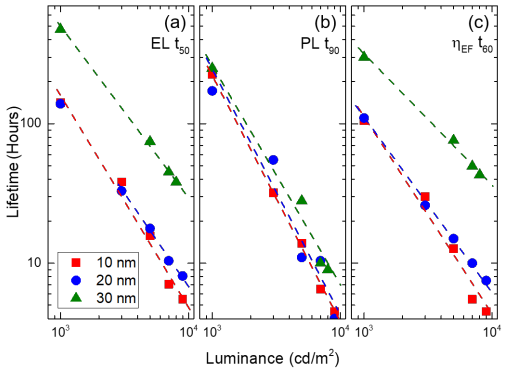

Figure 5.4: Extracted lifetimes for all 3 architecures as a function of luminance.

Chapter 6

Novel Blue Emitter Developement

6.1 Molecular Systems

6.2 Performance Optimization

6.3 Solution Molecular Aggregation

Chapter 7

Data Management for Devices

Chapter 8

Modeling Out-Coupling

8.1 Theory

8.2 Recombination Zone Overlap During Lifetime

Chapter 9

Future Research

Bibliography

[1] Hershey, K. W., and Cottingham, J. P. Material properties of pipes and reeds from the Southeast Asian khaen. *The Journal of the Acoustical Society of America 129*, 4 (apr 2011), 2520–2520.

[2] Hershey, K. W., and Holmes, R. J. Unified analysis of transient and steady-state electrophosphorescence using exciton and polaron dynamics modeling. *Journal of Applied Physics 120*, 19 (2016), 195501.

[3] Hershey, K. W., Suddard-Bangsund, J., Qian, G., and Holmes, R. J. Decoupling degradation in exciton formation and recombination during lifetime testing of organic light-emitting devices. *Applied Physics Letters 111*, 11 (2017), 113301.

[4] Xu, F., Hershey, K. W., Holmes, R. J., and Hoye, T. R. Blue-Emitting Arylalkynyl Naphthalene Derivatives via a Hexadehydro-Diels?Alder Cascade Reaction. *Journal of the American Chemical Society 138*, 39 (oct 2016), 12739–12742.

Appendices

Appendix A

List of Publications

- Hershey, K. W., and Cottingham, J. P. Material properties of pipes and reeds from the Southeast Asian khaen. *The Journal of the Acoustical Society of America 129*, 4 (apr 2011), 2520–2520
- Hershey, K. W., and Holmes, R. J. Unified analysis of transient and steady-state electrophosphorescence using exciton and polaron dynamics modeling. *Journal of Applied Physics 120*, 19 (2016), 195501
- Hershey, K. W., Suddard-Bangsund, J., Qian, G., and Holmes, R. J. Decoupling degradation in exciton formation and recombination during lifetime testing of organic light-emitting devices. *Applied Physics Letters 111*, 11 (2017), 113301
- Xu, F., Hershey, K. W., Holmes, R. J., and Hoye, T. R. Blue-Emitting Arylalkynyl Naphthalene Derivatives via a Hexadehydro-Diels?Alder Cascade Reaction. *Journal of the American Chemical Society 138*, 39 (oct 2016), 12739–12742

A.1 Measuring Triplet Energies

Appendix B

Out-Coupling Code

Appendix C

Lifetime Box Code

List of Figures

List of Tables